NOTE

Relationship between electron density and effective densities of body tissues for stopping, scattering and nuclear interaction of proton and ion beams

Nobuyuki Kanematsu[1,2]

[1] Department of Accelerator and Medical Physics, Research Center for Charged Particle Therapy, National Institute of Radiological Sciences, 4-9-1 Anagawa, Inage-ku, Chiba 263-8555, Japan

[2] Department of Quantum Science and Energy Engineering, School of Engineering, Tohoku University, 6-6 Aramaki Aza Aoba, Aoba-ku, Sendai 980-8579, Japan

E-mail: nkanemat@nirs.go.jp

Abstract. In treatment planning of charged-particle radiotherapy, patient heterogeneity is normally modeled as variable-density water to best reproduce the stopping power. This water-based model would cause substantial errors in multiple scattering and nuclear interaction as body tissues may deviate from water in elemental compositions. In this study, we physically defined distinctive effective densities for stopping, scattering, and nuclear interactions of proton and ions and constructed their conversion functions to correct the water-based model, using the standard elemental composition data for body tissues. As we took the electron density for the reference in the formulation, these conversion functions are generally valid for treatment planning systems that normally have a function to convert CT number to electron density or stopping-power ratio. The proposed extension in heterogeneity correction will enable accurate beam dose calculation without seriously sacrificing simplicity or efficiency of the water-based model.

PACS numbers: 87.53.-j, 87.53.Kn, 87.55.D-

1. Introduction

In the present practice of radiotherapy treatment planning, patent-specific material information is obtained from x-ray CT images (Goitein 1978). The CT number given to each image pixel represents the x-ray attenuation coefficient of the material, from which the effective density for the treatment beam is estimated on the presumption of one-to-one correspondence. Taking water as the reference material, the effective density is defined as the thickness ratio of water to a material for an equivalent dosimetric effect, which is mainly determined by attenuation for photons or energy loss (stopping) for charged particles (Schneider *et al* 1996, Kanematsu *et al* 2003). In other words, the patients are modeled as variable-density water. In conventional beam-based algorithms, a beam in water is precisely modeled and the beam transport theory accounts for the density-heterogeneity effects (Eyges 1948, Gottschalk 2010).

Matsufuji *et al* (1998) studied the water-based patient model and found that the errors for a typical bone tissue of CT number of 1000 HU would be about -10% in multiple-scattering angle and -10.0% in mean free path of proton nuclear interaction (56.1 cm for 62.3 cm). Palmans and Verhaegen (2005) constructed a separate CT-number conversion for proton nuclear interaction and found that the nuclear interaction in tissues estimated with the conversion for stopping would cause 2–3% dose errors in Monte Carlo simulations.

Recent advances in computing technology have made Monte Carlo particle simulation available for dose calculation of proton and ion beams (Jiang and Paganetti 2004, Kase *et al* 2006), where the energy loss and the multiple scattering are modeled as continuous processes in the medium and the nuclear interaction is modeled as an elementary nucleus–nucleus collision. Schneider *et al* (2000) proposed a method to convert CT number into mass density and elemental weights of body tissues to fully utilize the power of the Monte Carlo method for treatment planning. Nevertheless, patient physiological changes, organ motion, and setup errors between CT imaging and treatment sessions remain as uncertainties. Ideally, adaptive radiotherapy with in-situ CT imaging and replanning will reduce such errors (Yan *et al* 1997). Alternatively and palliatively, robust optimization techniques will mitigate their influence, but may increase the calculation time significantly (Unkelbach *et al* 2009, Inaniwa *et al* 2011). Deterministic algorithms are essential for those speed-demanding applications.

This study aims to extend the water-based model by introducing distinctive effective densities for stopping, scattering, and nuclear interaction of proton and ion beams, with which these interactions can be addressed accurately and efficiently. As the conversion from CT number to electron density is a common function of treatment planning systems, this study focuses on conversions from electron density to the other effective densities, which are irrelevant to individual CT systems.

2. Materials and methods

2.1. The ICRU body tissues

ICRU (1992) reported elemental compositions, mass density, and electron density of 106 materials of body tissues and ingredients, which have been repeatedly used for patient-modeling purposes (Matsufuji *et al* 1998, Schneider *et al* 2000, Kanematsu *et al* 2003, Palmans and Verhaegen 2005). In this study, we used 92 of them to represent human body tissues excluding obsolete and extreme materials such as ICRU-33 soft tissue, hydroxyapatite, calcifications, water, lipid, carbohydrate, cell nucleus, cholesterol, protein, and urinary stones. The electron density is calculated as

$$\rho_{\mathrm{e}} = \frac{\rho}{0.5551} \sum_i Z_i \frac{w_i}{A_{\mathrm{r}i}}, \tag{1}$$

where the Z_i and the $A_{\mathrm{r}i}$ are the atomic number and the atomic weight of element i, the w_i and the ρ are the elemental mass fraction and the mass density of the material, and the 0.5551 is the effective Z/A_{r} of water with mass fractions H:11.19% and O:88.81%.

2.2. Stopping

The Bethe theory (ICRU 1993) leads the stopping-power ratio of the material to water, or the stopping effective density, to

$$\rho_{\mathrm{S}} = \rho_{\mathrm{e}} \left(-\ln \frac{I}{m_{\mathrm{e}} c^2} + \ln \frac{2v^2}{c^2 - v^2} - \frac{v^2}{c^2} \right) \left(-\ln \frac{I_{\mathrm{w}}}{m_{\mathrm{e}} c^2} + \ln \frac{2v^2}{c^2 - v^2} - \frac{v^2}{c^2} \right)^{-1} \tag{2}$$

where $m_\mathrm{e} = 0.511\ \mathrm{MeV}/c^2$ is the electron mass, v and c are the speeds of the projectile and light, and I and $I_\mathrm{w} = 78$ eV (Sigmund *et al* 2009) are the mean excitation energies of the material and water. As a body tissue is a mixture of solid or liquid compounds, the mean excitation energy is calculated by the Bragg rule

$$\ln I = \sum_i \frac{w_i}{A_{\mathrm{r}i}} Z_i \ln I_i \left(\sum_i \frac{w_i}{A_{\mathrm{r}i}} Z_i \right)^{-1} \tag{3}$$

with constituent elemental I_i/eV values H:19.2, C:81, N:82, O:106, F:112, Na:168, Mg:176, P:195, Cl:180, K:215, Ca:216, and Fe:323 (ICRU 1984). As the v-dependent variation of the ρ_S is within 1% under therapeutic conditions (Kanematsu *et al* 2003), we take the representative projectile speed $v = 0.6\,c$ or the nucleon kinetic energy $E/A = 230$ MeV to define the stopping effective density as projectile independent.

2.3. Scattering

Gottschalk (2010) proposed a material property, the scattering length, for multiple scattering of heavy particles. For a material of single element i, the scattering mass length $X_{\mathrm{T}i}$ in units of g/cm^2 is formulated as

$$\frac{1}{X_{\mathrm{T}i}} = \frac{1}{2865.6\ \mathrm{g/cm^2}} \frac{Z_i^2}{A_{\mathrm{r}i}} \left(\frac{2}{3} \ln \frac{36.657 \times 10^{12}}{A_{\mathrm{r}i} Z_i} - 1 \right). \tag{4}$$

The scattering mass length of a composite material, X_T, is given by $1/X_\mathrm{T} = \sum_i w_i/X_{\mathrm{T}i}$, for example, 46.88 g/cm^2 for water. The scattering power T is inversely proportional to the scattering length X_T/ρ. The scattering-power ratio of the material to water, or the scattering effective density, is thus formulated as

$$\rho_\mathrm{T} = \frac{\rho}{61.122} \sum_i \frac{w_i}{A_{\mathrm{r}i}} Z_i^2 \left(\frac{2}{3} \ln \frac{36.657 \times 10^{12}}{A_{\mathrm{r}i} Z_i} - 1 \right). \tag{5}$$

2.4. Nuclear interaction

Sihver *et al* (1993) made empirical modification to the geometric model for nucleus–nucleus collision cross section as

$$\sigma_\mathrm{N} = \pi r_0^2 \left[A^{1/3} + A_\mathrm{r}^{1/3} - b_0 \left(A^{-1/3} + A_\mathrm{r}^{-1/3} \right) \right]^2, \tag{6}$$

$$b_0 = \begin{cases} 2.247 - 0.915 \left(1 + A_\mathrm{r}^{-1/3} \right) & \text{for protons} \\ 1.581 - 0.876 \left(A^{-1/3} + A_\mathrm{r}^{-1/3} \right) & \text{for ions} \end{cases} \tag{7}$$

where we consistently used symbols A for mass number of the projectile and A_r for atomic weight of the target and introduced $r_0 = 1.36$ fm for effective nucleon radius and b_0 for overlap parameter. In their recent formulation (Sihver and Mancusi 2009), the energy-dependent factor is insensitive to target nuclei at therapeutic energies ($E/A > 120$ MeV) and is thus disregarded in this study. The mean atomic weight $\overline{A}_\mathrm{r}$ and the mean nuclear cross section $\overline{\sigma}_\mathrm{N}$ of a compound or mixture are defined as,

$$\overline{A}_\mathrm{r} = \left(\sum_i \frac{w_i}{A_{\mathrm{r}i}} \right)^{-1}, \tag{8}$$

$$\overline{\sigma}_\mathrm{N} = \pi r_0^2 \sum_i \left(A^{1/3} + {A_{\mathrm{r}i}}^{1/3} - b_0 \right)^2 \frac{w_i}{A_{\mathrm{r}i}} \overline{A}_\mathrm{r}. \tag{9}$$

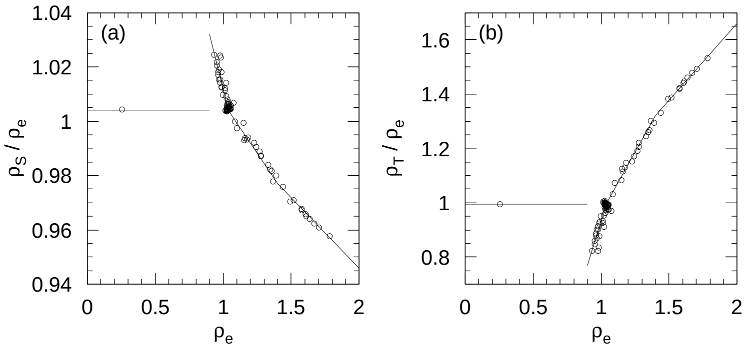

Figure 1. Ratios of (a) stopping effective density ρ_{S} and (b) scattering effective density ρ_{T} to electron density ρ_{e} of body tissues for proton and ion beams with the conversion polylines as a function of ρ_{e}.

Table 1. Conversion factors from electron density ρ_{e} to stopping effective density ρ_{S} and scattering effective density ρ_{T}.

ρ_{e}	0	0.9	0.9	1.035	1.4	2.0
$\rho_{\mathrm{S}}/\rho_{\mathrm{e}}$	1.004	1.004	1.032	1.004	0.977	0.946
$\rho_{\mathrm{T}}/\rho_{\mathrm{e}}$	0.995	0.995	0.77	0.995	1.32	1.66

The nuclear effective density ρ_{N} is proportional to the mass density ρ and the mean nuclear cross section per mass, $\overline{\sigma}_{\mathrm{N}}/\overline{A}_{\mathrm{r}}$, and is normalized to 1 for water, namely

$$\rho_{\mathrm{N}} = \rho\,\frac{\overline{\sigma}_{\mathrm{N}}}{\overline{\sigma}_{\mathrm{Nw}}}\,\frac{\overline{A}_{\mathrm{rw}}}{\overline{A}_{\mathrm{r}}}, \tag{10}$$

where the $\overline{\sigma}_{\mathrm{Nw}}$ and the $\overline{A}_{\mathrm{rw}}$ are the mean nuclear cross section and the mean atomic weight of water. Unlike the other effective densities, we formulated the nuclear effective density as projectile dependent.

3. Results

Figure 1 shows the correspondences between the electron density and the stopping and scattering effective densities for proton and ion beams. There was a high concentration of tissues around $(\rho_{\mathrm{e}}, \rho_{\mathrm{S}}/\rho_{\mathrm{e}}, \rho_{\mathrm{T}}/\rho_{\mathrm{e}}) = (1.035, 1.004, 0.995)$. The low $\rho_{\mathrm{e}} = 0.258$ for the lung tissue was attributed to the air content and thus the ratios $\rho_{\mathrm{S}}/\rho_{\mathrm{e}}$ and $\rho_{\mathrm{T}}/\rho_{\mathrm{e}}$, namely the conversion factors, should be invariant in the low ρ_{e} region. Otherwise, the negative correlation between $\rho_{\mathrm{S}}/\rho_{\mathrm{e}}$ and ρ_{e} reflected low I values of carbon-rich adipose tissues in the low ρ_{e} region and high I values of calcium-rich bone tissues in the high ρ_{e} region. The positive correlation between $\rho_{\mathrm{T}}/\rho_{\mathrm{e}}$ and ρ_{e} reflected the Z^2 dependence of Coulomb scattering against the Z^1 dependence of the ρ_{e}. For the conversion functions, we set a discontinuity point at $\rho_{\mathrm{e}} = 0.9$, where none of these tissues are present, an inflection point at the center of the concentration, and another inflection point at $\rho_{\mathrm{e}} = 1.4$ for bone tissues. Table 1 shows the resultant conversion factors defined as polyline functions.

Figure 2 shows the correspondences between the electron density and the nuclear effective densities for protons, helium ions, carbon ions, and oxygen ions. The $\rho_{\mathrm{N}}/\rho_{\mathrm{e}}$

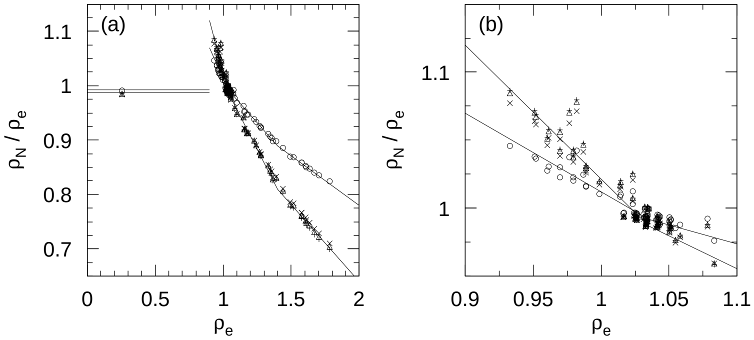

Figure 2. (a) Ratios of nuclear effective density ρ_N for protons (∘), helium ions (×), carbon ions (△), and oxygen ions (+) to electron density ρ_e with the conversion lines as a function of ρ_e and (b) an enlarged view.

Table 2. Conversion factors from electron density ρ_e to nuclear effective density ρ_N for protons and ions of $4 \leq A \leq 16$.

ρ_e	0	0.9	0.9	1.035	1.4	2.0
$\rho_\mathrm{N}/\rho_\mathrm{e}$ for protons	0.992	0.992	1.07	0.992	0.89	0.78
$\rho_\mathrm{N}/\rho_\mathrm{e}$ for ions	0.987	0.987	1.12	0.987	0.81	0.64

Table 3. Mean nuclear cross section of water, $\overline{\sigma}_\mathrm{N\,w}$, for protons, helium ions, carbon ions, and oxygen ions, in units of $\pi\, r_0^2 = 5.81$ fm^2.

Projectile	protons	He ions	C ions	O ions
$\overline{\sigma}_\mathrm{N\,w}/(\pi\, r_0^2)$	2.47	7.51	10.93	12.35

ratio for protons largely deviated from those for the ions mainly due to the distinctive formulation of the overlap parameter b_0 in (7). The negative correlation between $\rho_\mathrm{N}/\rho_\mathrm{e}$ and ρ_e reflected the approximate $A_\mathrm{r}^{2/3}$ dependence of the nuclear cross section against the approximate A_r^1 dependence of the ρ_e. As the variation among the ions is rather smaller than the variation among the tissues of similar ρ_e, it may be reasonable to have one conversion function for the ions of $4 \leq A \leq 16$ in addition to that for protons. Table 2 shows the resultant conversion factors that were similarly defined as polyline functions. Nevertheless, the frequency of nuclear interaction varies among the projectiles as shown in table 3.

4. Discussion

Matsufuji *et al* (1998) assumed that the electron density ρ_e would be a fair approximation to the stopping effective density ρ_S. In fact, the conversion factor $\rho_\mathrm{S}/\rho_\mathrm{e}$ deviated from 1 by up to a few percent. They also related the CT number of 1000 HU with $\rho_\mathrm{e} \approx 1.35$, which would convert into $\rho_\mathrm{T} = 1.21\,\rho_\mathrm{e}$ using table 1 and $\rho_\mathrm{N} = 0.904\,\rho_\mathrm{e}$ for protons using table 2. As the multiple-scattering angle is proportional to $\sqrt{\rho_\mathrm{T}}$ and the mean free path is proportional to $1/\rho_\mathrm{N}$, these conversions would correct the scattering-angle error of −9.1% and the mean-free-path error of −9.6% in the uncorrected water-based model, which may be consistent with their original estimations of about −10% and −10.0%, respectively.

In treatment planning with the water-based model, an elementary beam in water must be modeled and used with sufficient accuracy and efficiency. For stopping, the relation between energy E and in-water range R is readily available in forms of tables (Janni 1982, ICRU 1993, Sigmund *et al* 2009) and approximate formulas (Bortfeld 1997, Kanematsu 2008). For multiple scattering, Kanematsu (2009) proposed a simple scattering-power formula to address heterogeneity. Those beam models are sufficiently accurate and efficient for treatment planning (Kanematsu 2011).

Unlike the stopping and scattering processes, the nuclear interaction causes attenuation of the primary particles and yield of projectile and target fragments. Janni (1982) tabulated the projectile proton loss, with which Lee *et al* (1993) proposed an approximation formula for fluence $\Phi(R) \approx \Phi(0)\,(1 + 0.012R/\mathrm{cm})$ as a linear function of residual range R. Matsufuji *et al* (2003) measured projectile carbon-ion fluence in PMMA (H:8.05%, C:59.98%, O:31.96%), which also showed approximate linear attenuation to about a half at the range of 14 cm. With small correction for PMMA ($\rho_\mathrm{N}/\rho_\mathrm{S} = 0.962$), the carbon-ion fluence formula would be $\Phi(R) \approx \Phi(0)\,(1 + 0.07R/\mathrm{cm})$.

The fragmentation processes are complex and the biological effectiveness of absorbed dose varies among the fragments and their energies, which make their modeling very challenging. Even for protons, where projectile fragments are absent, target fragments contribute to therapeutic dose substantially (Paganetti 2005). In the participant–spectator model (Baur *et al* 1984), the target will not directly influence how the projectile may break up. The relative yields of projectile fragments (Matsufuji *et al* 2003) may thus be reasonably invariant to target materials, which also justifies the water-based modeling. Due to experimental difficulties in precise measurement of a treatment-beam spectrum, Monte Carlo simulation will be useful to build a detailed beam model in numerical or analytical form (Kempe and Brahme 2010).

5. Conclusions

For general body tissues, there are strong correlations between electron density and effective densities that characterize the strengths of stopping, scattering, and nuclear interactions of the projectile protons and ions. The stopping effective density deviated from the electron density by up to a few percent. The scattering and nuclear effective densities deviated by up to a few tens percent, which were consistent with other studies. To correct those errors, distinctive conversion functions from electron density into the effective densities were defined, where the electron density may be conventionally derived from x-ray CT number. The proposed extension in heterogeneity correction will enable accurate beam dose calculation without seriously sacrificing simplicity or efficiency of the water-based model.

References

Baur G, Rössel F, Trautmann D and Shyam R 1984 Fragmentation processes in nuclear reactions *Phys. Rep.* **111** 333–71

Bortfeld T 1997 An analytical approximation of the Bragg curve for therapeutic proton beams *Med. Phys.* **24** 2024–33

Eyges L 1948 Multiple scattering with energy loss *Phys. Rev.* **74** 1534–5

Goitein M 1978 Compensation for inhomogeneities in charged particle radiotherapy using computed tomography *Int. J. Radiat. Oncol. Biol. Phys.* **4** 499–508

Gottschalk B 2010 On the scattering power of radiotherapy protons *Med. Phys.* **37** 352–367

ICRU 1984 Stopping powers for electrons and positrons *ICRU Report* 37 (Bethesda, MD: ICRU)

ICRU 1992 Photon, electron, proton and neutron interaction data for body tissues *ICRU Report* 46 (Bethesda, MD: ICRU)

ICRU 1993 Stopping powers and ranges for protons and alpha particles *ICRU Report* 49 (Bethesda, MD: ICRU)

Janni J F 1982 Proton range–energy tables 1 keV–10 GeV *Atomic Data and Nuclear Data Tables* **27** 147–339

Jiang H and Paganetti H 2004 Adaptation of GEANT4 to Monte Carlo dose calculations based on CT data *Med. Phys.* **31** 2811–8

Kanematsu N, Matsufuji N, Kohno R, Minohara S and Kanai T 2003 A CT calibration method based on the polybinary tissue model for radiotherapy treatment planning *Phys. Med. Biol.* **48** 1053–64

Kanematsu N 2008 Alternative scattering power for Gaussian beam model of heavy charged particles *Nucl. Instrum. Methods B* **266** 5056–62

Kanematsu N 2009 Semi-empirical formulation of multiple scattering for the Gaussian beam model of heavy charged particles stopping in tissue-like matter *Phys. Med. Biol.* **54** N67–73

Kanematsu N 2011 Dose calculation algorithm of fast fine-heterogeneity correction for heavy charged particle radiotherapy *Physica Medica* **27** 97–102

Kase Y, Kanematsu N, Kanai T and Matsufuji N 2006 Biological dose calculation with Monte Carlo physics simulation for heavy-ion radiotherapy *Phys. Med. Biol.* **51** N467–75

Kempe J and Brahme A 2010 Analytical theory for the fluence, planar fluence, energy fluence, planar energy fluence and absorbed dose of primary particles and their fragments in broad therapeutic light ion beams . *Physica Medica* **26** 6–16

Lee M, Nahum A E and Webb S 1993 An empirical method to build up a model of proton dose distribution for a radiotherapy treatment-planning package *Phys. Med. Biol.* **38** 989–98

Matsufuji N, Tomura H, Futami Y, Yamashita H, Higashi A, Minohara S, Endo M and Kanai T 1998 Relationship between CT number and electron density, scatter angle and nuclear reaction for hadron-therapy treatment planning *Phys. Med. Biol.* **43** 3261–75

Matsufuji N, Fukumura A, Komori M, Kanai T and Kohno T 2003 Influence of fragment reaction of relativistic heavy charged particles on heavy-ion radiotherapy *Phys. Med. Biol.* **48** 1605–23

Paganetti H 2005 Nuclear interactions in proton therapy: dose and relative biological effect distributions originating from primary and secondary particles *Phys. Med. Biol.* **50** 991-1000

Palmans H and Verhaegen F 2005 Assigning nonelastic nuclear interaction cross sections to Hounsfield units for Monte Carlo treatment planning of proton beams *Phys. Med. Biol.* **50** 991–1000

Schneider W, Bortfeld T and Schlegel W 2000 Correlation between CT numbers and tissue parameters needed for Monte Carlo simulations of clinical dose distributions *Phys. Med. Biol.* **45** 459–78

Sigmund P, Schinner A and Paul H 2009 Errata and addenda for ICRU Report 73, stopping of ions heavier than helium *Journal of the ICRU* **5**

Sihver L, Tsao C H, Silberberg R, Kanai T and Barghouty A F 1993 Total reaction and partial cross section calculations in proton–nucleus ($Z_t \leq 26$) and nucleus–nucleus reactions ($Z_p and Z_t \leq 26$) *Phys, Rev. C* **47** 1225–36

Sihver Land Mancusi D 2009 Present status and validation of `HIBRAC` *Radiation Measurements* **44** 38–46

Unkelbach J, Bortfeld T, Martin B C and Soukup M 2009 Reducing the sensitivity of IMPT treatment plans to setup and range uncertainties via probabilistic treatment planning *Med. Phys.* **36** 149–63

Yan D, Vicini F, Wong J and Martinez A 1997 Adaptive radiation therapy *Phys. Med. Biol.* **42** 123–32